Indian Journal of Engineering & Materials Sciences
Vol. 31, June 2024, pp. 397-404
DOI: 10.56042/ijems.v31i3.6628

Optimization and property evaluation of 0.5 mm SS304 thick sheets welded by microplasma arc welding with and without post heat treatment

Kasif Ansari & Mayuri Baruah*

Production and IndustrialEngineering Department, National Institute of Technology Jamshedpur, Jharkhand 831014, India

Received: 07 November 2023; Accepted: 02 April 2024

The present work investigates the micro plasma arc welding (MPAW) of SS304L of 0.5 mm steel sheets. It primarily highlights the weld quality of SS304 of 0.5 mm thickness with and without post weld heat treatment (PWHT). Thin sheets are more prone to distortion at time of solidification because of residual stress induced. After PWHT of the welded sample, the distortion is reduced. The effect of input parameters such as pulse current, gas flow rate and welding speed are taken into consideration. Property evaluation and comparison of weld are carried out before and after the PWHT by hardness, tensile test, microstructure, X-Ray Diffraction (XRD) and scanning electron microscope (SEM). Furthermore, artificial neural network (ANN) is applied for optimization of the weld quality at chosen process parameters and compared to that of the experimental results by considering tensile strength as an output. The ANN will be useful for estimating the welding current to yield an optimum tensile strength, thus providing better process control.

Keywords: Micro plasma arc welding (MPAW), Distortion, Artificial neural network (ANN), Residual stress, Post weld heat treatment (PWHT)

1 Introduction

Miniaturization is the new trend adopted in the industries in the recent years.This led to the reduced resource/fuel consumption along with reduced weight of the component. Techniques to join or assemble small/thin components are increasingly being explored and investigated. Microplasmaarc welding (MPAW) is one such technique which has the capability of forming very small thermally effected as the heat input can be controlled to very small value[1]. This makes the technique suitable for fabricating very thin sheets. However, with reduced thickness, the problem of distortion and bending increases as huge temperature gradient exists in a small area. Thus, in depth insight into the underlying physics and apt process optimization is an important requisite for defect less fabrication[2]. In this current study, the microplasma arc welding technique is explored for joining sstainless steel sheets. Principle of MPAW is similar to Tungsten inert gas (TIG) welding except for the electrode which is kept inside the nozzle so that intense heat is generated which can be focussed to a small area and thus, there is low heat affected zone (HAZ)[3]. Additionally, MPAW has some other extensive properties such as fast welding speed, high mechanical strength, and low distortion[4]. Though LASER technique is found to produce quality joints of thin sheets of stainless steel 304 (SS304) sheets[5]. However, portable and compact equipment of MPAW along with low cost makes it a preferable choice for joining such materials over LASER technique.

SS304 is a common austenitic stainless steel and it is mainly used in petroleum, chemical and metallurgical and automobile industries as it has good resistance to high temperature oxidation, crakes, pitting and stress corrosion cracking[6]. Various researchers are investigating the MPAW of SS304. Compared to other arc welding processes, coarsening of the grain at HAZ and cooling rate is slower in MPAW[7].The formation of secondary phase particles, such as the sigma phase that occurs in weld metal and HAZis another issue that emerges at the joint of ferritic stainless steels, in addition to the coarsening of the grain[8]. Creation of secondary phase in the welding zone deteriorates the weldjoint properties like hardness, tensile strength and ductility[9]. It is found that post weld heat treatment (PWHT) of the fabricated samples as well as apt process optimization may somewhat improve the quality of the joints[10].

Lin et al.[11] performed the PWHT of D6AC steel and concluded that fatigue crack growth decreases with an increasein tempering temperature. Panov et

*Corresponding author (E-mail: k.ansari251@gmail.com)

al.[12] studied effect of PWHT found that there is a formation of a course columnar structure in B-phase form at the fusion zone (FZ) which results in decrease in strength and microhardness at the FZ. Haigen *et al.*[13] also performed experiments on dissimilar materials and concluded that after PWHT, tensile strength and microstructure improved. From literature, it is found that PWHT of the welded joints enhances their properties. These heat treatments increase the ferritic stainless steel welds' tensile strength, ductility, and ability to resist corrosion. The PWHT done between 700°C-900°C tempered the martensite, reduced the residual stress and had little effect on the microstructure[14]. This heat treatment reformed the austenite. However,a decrease in ductility and/or toughness, and grain coarsening at HAZis observed. Fatima et al.[15]investigated about optimization of process parameter for fabrication of dissimilar material SS304 and low carbon steel by MPAW for the welding quality.Pal et al.[16] developed an artificial neural network (ANN) model to select optimum welding parameters such as gas flow rate, welding voltage and welding current for required output specifications.

In the present work, MPAW of 0.5 mm thin sheets are performed at various welding currents with all other parameters constant. After successful weld joint fabrication, post heat treatment is carried out to study its effect on the properties of the joints. The weld joints are then evaluated by tensile strength, microstructure and hardness before and after PWHT. The impact of PWHT on mechanical characteristics, microstructure and hardness is then investigated. Furthermore, an artificial neural network (ANN) is applied for optimization of the weld quality choosing tensile strength as an output at chosen process parameters and compared to that of the experimental results.

2 Materials and Methods

2.1 Materials and Methodology

Microplasma arc welding (MPAW) is performed to join thin steel sheets in this present study. The MPAW machine used is shown in Fig. 1(a). The welding torch used is fixed vertically in such a way that distance is maintained between the workpiece and nozzle. A fixture, made of copper, is used to hold the workpiece so as to ensure no warpage and deformation in the sheets during welding. The experimental setup indicating fixture setup along with torch holder is shown in the figure 1(b). The process parameters are depicted in Table 1.

The present work represents similar joining of Stainless steel 304 (SS304) with dimension 150mm × 100mm × 0.5 mm used as a workpiece. Weight

Table 1— MPAW process parameters used for the experimentation

Welding Parameters	Values
Rate of flow of main gas for welding	3.5 Lpm
Welding speed	4.2 mm/s
Welding Current	8 -12 A
Shielding gas flow rate	0.4 Lpm
Torch Position	Vertical
Electrode diameter	1.2 mm
Copper Nozzle diameter	1.2 mm
Nozzle to plate distance	2 mm

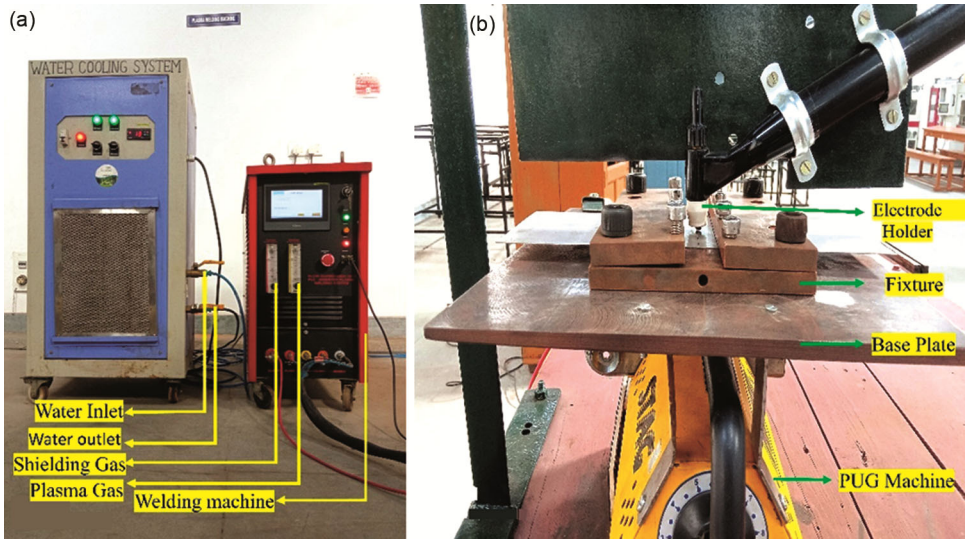

Fig. 1 — (a) Welding machine, and (b) Welding setup along with the torch and fixture arrangement.

percentage of chemical composition of SS304 is charted in the Table 2 and tested using X-ray photoelectron spectroscopy. The workpiece is cleaned by emery paper and acetone to remove impurities at the welding edge. After edge preparation workpieces are tightly hold in the fixture in such a way that nozzle tip is able to move exactly on top of the butt line between the work pieces at a fixed arc length. After series of iterative trials, stable welding zone is ascertained for having full penetration and having no visible weld defects. Figure 2 shows the welding samples at various welding current with all other process parameters remaining constant.

2.2 Post heat treatment

For the enhancement of microstructure and mechanical properties, PWHT is performed at 300°C-400°C in the interval of 50°C. After maintaining at this temperature for 0.75h to 1h, the specimen is quenched in water which is shown in the Fig. 3.

2.3 Modelling of the MPAW

Multiple regression analysis and an artificial neural network are two of the modelling methods used in this paper.

Table 2 — Chemical composition of stainless steel 304L (Weight %)

Elements	Fe	C	Ni	Cr	Si	Mn	P	S	Mo
Contents	Bal.	0.023	8.27	19.01	0.36	1.54	0.001	0.01	0.305

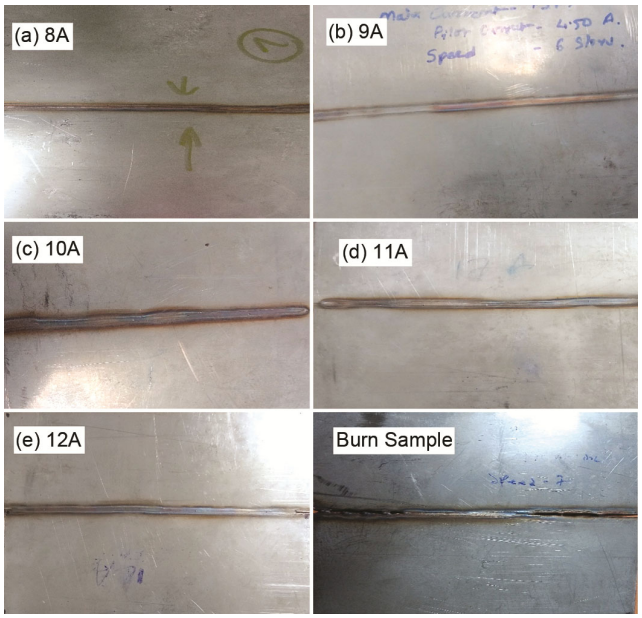

Fig. 2 — Schematic diagram of welded sample at (a) 8A current, (b) 9A current, (c) 10A current, (d) 11A current, and (e) 12A current and other process parameter constant.

2.3.1 Artificial Neural Network (ANN) modelling

Artificial Neural Network (ANN) is one such models which has found its niche in various applications for accurate monitoring of manufacturing processes, weather forecasting, sales forecasting, medicine, finance, speech recognition and pattern recognition. These applications deal with highly interactive and complex processes. This method has the benefit of allowing the model to use experimental data without any simplifying assumptions.Different types of ANN, including self-organizing maps (SOM), radial basis functions (RBF), and multilayer perception (MLP), are used in modelling. However, MLP is frequently utilised in weld modelling and is typically trained utilising the back propagation error approach[17]. The current investigation deals with MPAW process for optimization of the welding current having an optimum tensile strength of the fabricated joint. A code is developed in C programming language for multi-neuron, multi hidden layered ANN model, the illustration of the back-propagation ANN architecture is presented in Fig. 4. The hidden layer and output layer neurons' trailing functions and adaption learning function are regarded as TRAINLM and LEARNGDM, respectively. The network consists a number of hidden layers in between an input layer and an output layer. The double hidden layer back-propagation neural networks (BPNN) utilised in this study have one neuron in the output layer, which stands in for tensile strength, and three nodes in the input layer, which stand in for gas flow rate, welding speed and welding current respectively. The study's variable parameter is the number of hidden layer neurons,

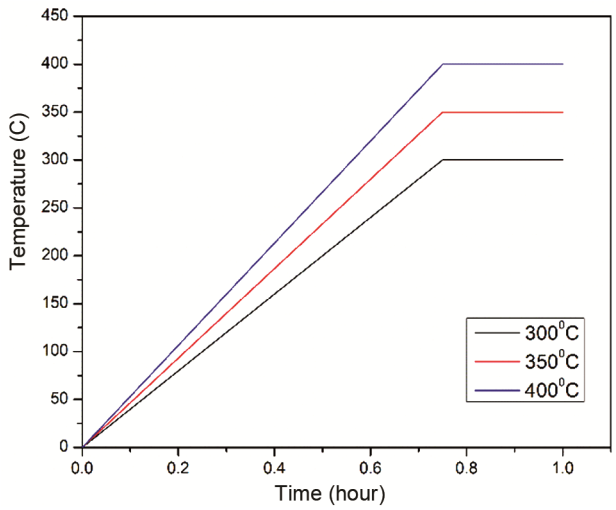

Fig. 3 — Schematic diagrams post-weld heat treatment schedules.

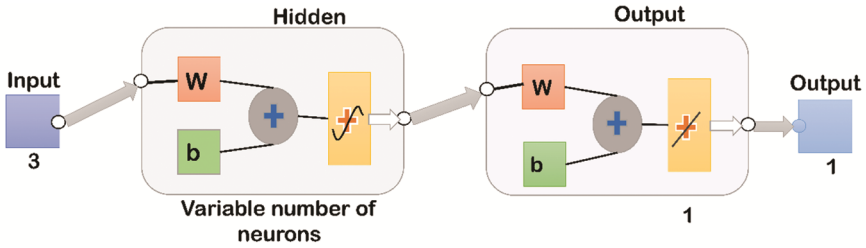

Fig. 4 — Schematic illustration of backpropagation ANN architecture.

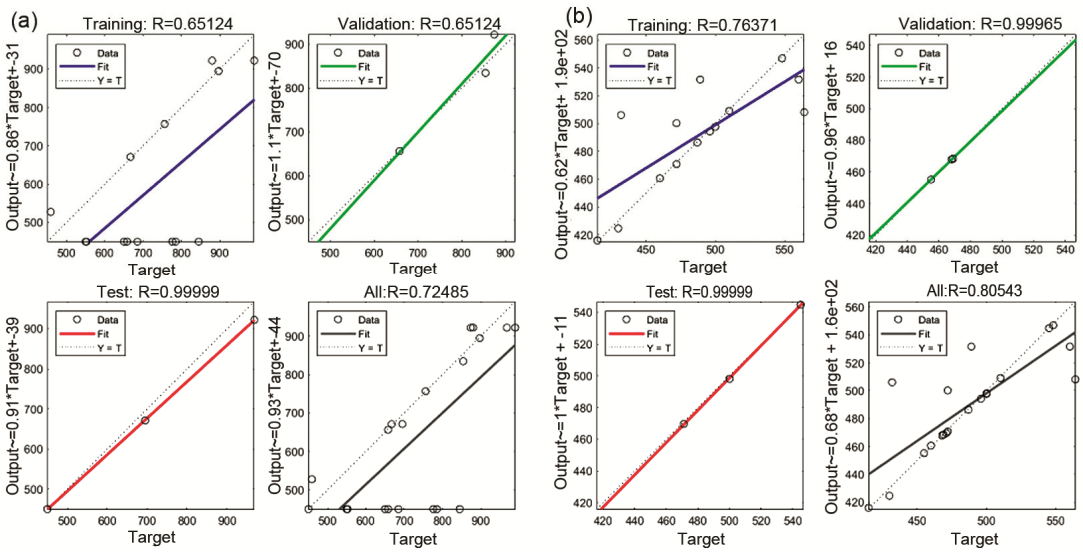

Fig. 5 — (a) Trailing, Testing and Validation graph of welded sample, and (b) Trailing, Testing and Validation graph of heat-treated welded sample.

which ranged from 5 to 15. All nodes in a layer are connected to all nodes in the next layers, and the number of neurons in each hidden layer and the number of hidden levels have both been changed. The input layer gets the data from an outside source, multiplies it by the interconnection weights with the neighbouring hidden layer, and then adds the results together. An activation function (in this example, sigmoid, a transfer function) modifies the summation of products, and the modified values then serve as the output signal for the first hidden layer and the input signal for the subsequent layer. Likewise, the signal finally enters the output layer, and terminates at the external receptor node(s). Using the error back-propagation technique the network is trained under supervision.

2.3.2 Training with radial basis neural network

Input and hidden layer do not have any weighted connections in radial basis neural networks (RBFN). Activation of hidden neuron is computed by using Gaussian basis unction as shown in equation 1. The Gaussian basis function which describes the signal function at the hidden neuron[7] as expressed in equation 1.

$$\varphi(\chi) = \exp\left(-\frac{\|\chi-\upsilon\|}{2\sigma^2}\right) \quad \ldots (1)$$

where υ is the centre of the training data points or the basis function and σ is the spread factor. These factors have direct effect on the smoothness of the interpolating function. Number of hidden layer neurons in RBFN with precise interpolator is equal to number of training data. As there are 20 training data points in the current problem (80% of the experimental data), there are 20 hidden layers with gaussian activation functions. The schematic diagram of back propagation ANN architecture shown in the Fig. 4.

2.3.3 Regression modelling of welding strength

Based on the experimental dataset, a multivariable regression model is created. In this work, relation between MPAW process parameters namely welding current (I), welding speed (V_w) and gas flow rate (f), and the process output specified as ultimate tensile strength (UTS) is examined. A linear model is first created and it is important to check the satisfactory

of the suggested model and regression coefficient (*R-square*) value of the regression equations.

$$\text{Tensile Strength} = 0.91 * \text{Target} + 39 \quad \ldots (2)$$

3 Results and Discussion

3.1 Distortion measurement

In the welding of thin sheets, the distortion is a major issue. In this investigation, the distortion of both before and after PWHT samples at 10 A current aremeasured by coordination measuring machine (CMM) which is presented in Fig. 6(a&b). Figure 7 shows that reducing the distortion of heat-treated welded sample which is measured in coordinate measuring machine (CMM).

Table 3 — Performance of BPNN with ANN network during testing using testing input data.

S. No.	Welding Current	Experimental Output	Output through ANN	Absolute % Error
1	8A	857	818.87	0.0442
2	9A	848	810.68	0.0440
3	10A	860	821.6	0.0461
4	11A	872	832.52	0.0452
5	12A	835	798.85	0.0432

Mean absolute % error = 0.04454

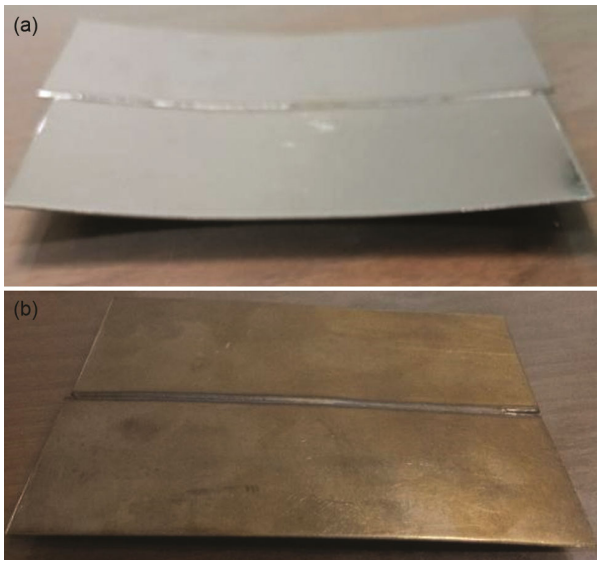

Fig. 6 — Distorted Sample at (a) Before PWHT, and (b) PWHT sample.

3.2 Ultimate Tensile Strength (UTS)

To prepare tensile weld specimens according to ASTM E8M-04 requirements, the weldments are cut in the transverse direction using wire cut electro discharge machining which is shown in the Fig. 8(a&b). The ultimate tensile strength is measured before and after the PWHT. The broken samples are shown in Figs 8(c&d). After PWHT the tensile strength and elongation percentage decreases due to presence of martensitic area precipitation of chromium carbide at the grain boundaries. From the Fig. 9 shows that tensile strength of heat-treated sample are reduced because some intermetallic compound are found. The tensile strength of welded samples before and after PWHT samples at 10A current which is shown in the Fig. 10. Tensile strength of base metal shown in the figure 10. Tensile strength of welded sample and heat treated sample at different process parameters.

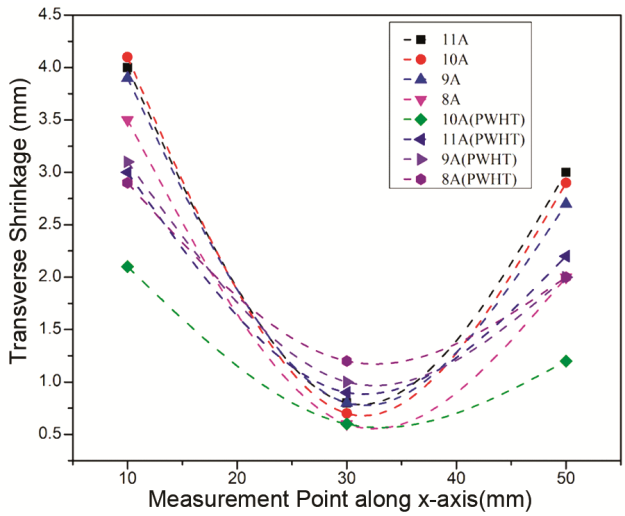

Fig. 7 — Distortion measurement of welded sample at different welding parameters with heat treated and without heat treated sample.

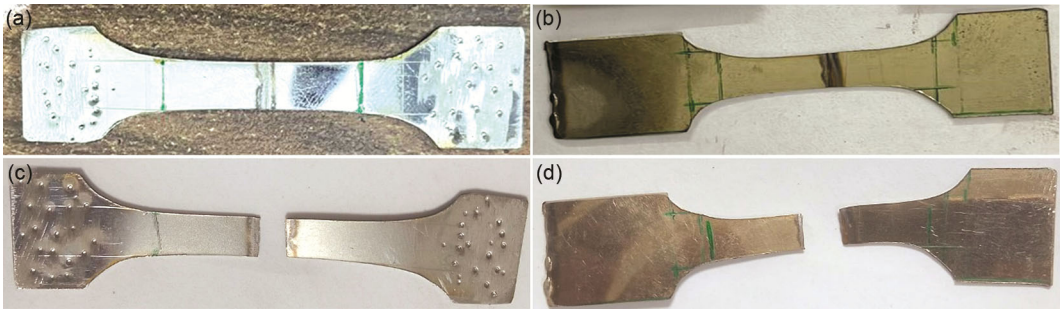

Fig. 8 — (a) Tensile Specimen before Heat treated, and (b) Tensile Specimen after Heat treated.

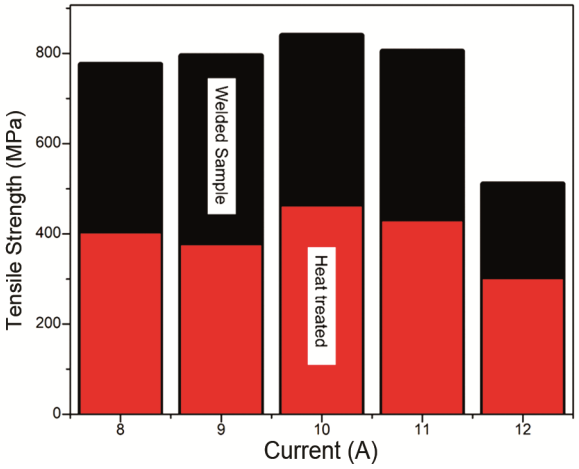

Fig. 9 — Tensile Strength of welded and heat treated sample at different current and welding speed.

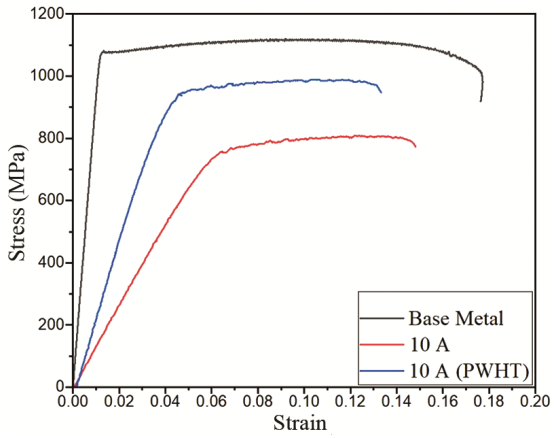

Fig. 10 — Tensile strength of base metal, welded and heat-treated welded sample (10 A and 3.5Lpm gas flow rate, 4.2mm/sec).

3.3 Measurement of hardness at fusion, HAZ and base metal one

Micro hardness testingis executed by Vickers hardness machine (machine: FIE-VMI) at the three different regionsi.e., base metal, HAZ and fusion zone on both side welded sample which shown in the Fig. 11. Hardness values were measured by applying the load 1 kg weight and d well time 10 second as per the ASTM E384-2017. The hardness valuesof welded samples at 10 Ameasured before and after the PWHT are shown in the figure 11. The figure depicts that hardness is highest at the FZ. It also indicates with an increase in the welding current, hardness value increased due to presence of martensitic precipitation of chromium carbide at the grain boundaries. After the PWHT, hardness is measured and its value is found greater than without heat treated weld sample. It is because after the heat

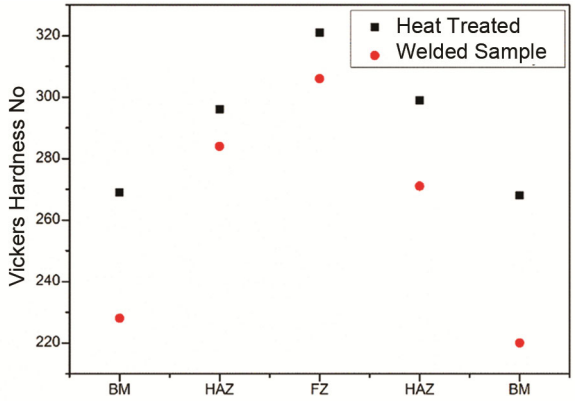

Fig. 11 — Hardness value welded and heat-treated welded sample at 10 A current.

treatment process quenching process is done for 5 seconds and columnar martensitic structure is formed at the FZ and also refinement of the grain occurred in the fusion zone.

3.4 Microstructure

The specimens were evaluated for microstructural analysis. The specimen is mounted by using Bakelite. The preparation of the sample and mounting is carried out according to the ASM Metal Handbook, Vol-09:2004 norms. The samples were polished by using emery paper of different grade (mesh size 425). Final polishing of samples is done with aluminium oxide and diamond paste. Polished sample are etched by carpenter Etchant solution. The microstructure of the base metal, weld zone and HAZ were analysed by optical microscope. Grain microstructure is presented in Figs 12 & 13 of before and after PWHT. From the Figs 12 & 13 grain refinement in the PWHT welded sample is seen. For evaluating the phases formed at different zones, XRD analysis is conducted which is depicted in Fig. 14. From Figure 14, it is revealed that the α-phase reduced with the heat-treated welded sample.

Figure 15 shows the SEM image of welded and heat-treated welded sample. The black particles in the base metal stainless steel 304 which is identified as carbides in the austenitic matrix. In the welded zone, martensite formation is seen in the FZ. Heat affected zone (HAZ) coarse grain are formed. There is a distinct microstructural variation between the weld zone and the HAZ. The two-phase transformation seen between HAZ and fusion zone (FZ) during the solidification time i.e., high temperature transformation of δ-Fe to γ-Fe and γ-Fe to α-Fe transformation.

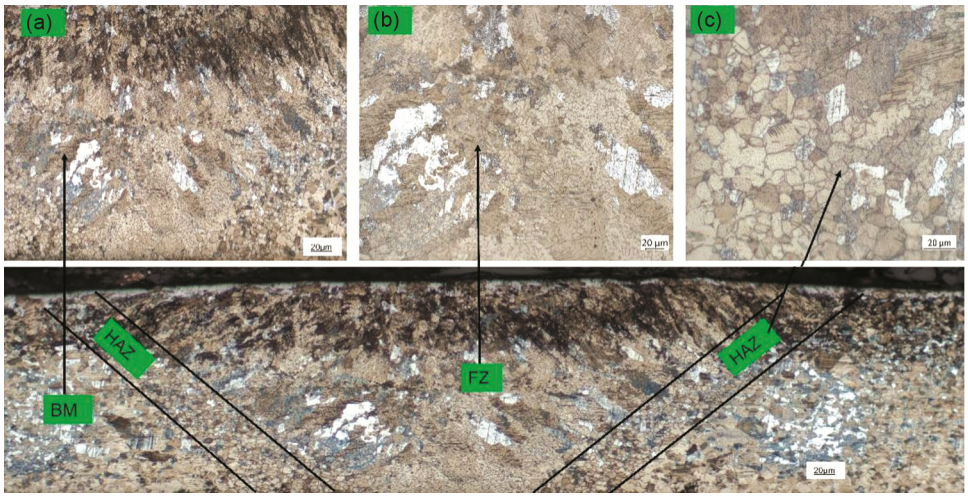

Fig. 12 — Microstructure of welded sample (a) Base zone, (b) FZ, and (c) HAZ.

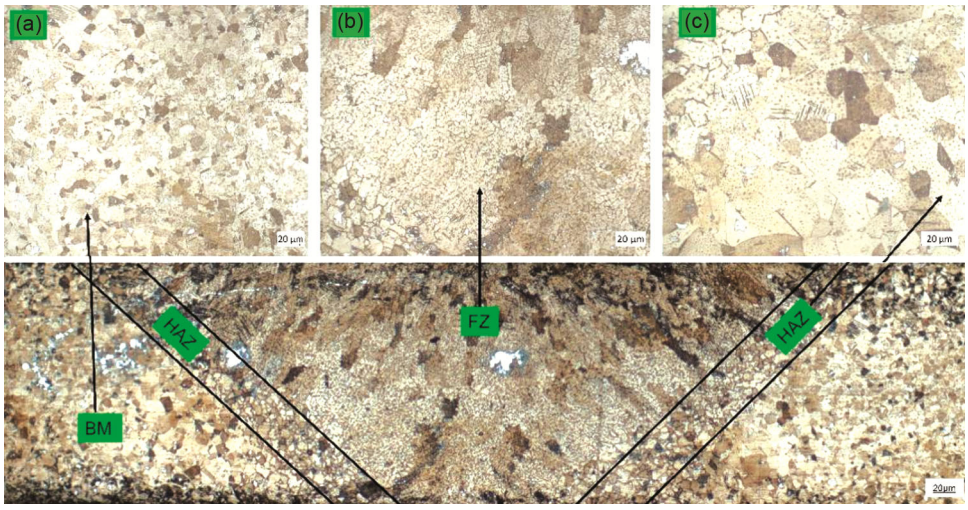

Fig. 13 — Microstructure of heat-treated welded sample (a) Base zone, (b) FZ, and (c) HAZ.

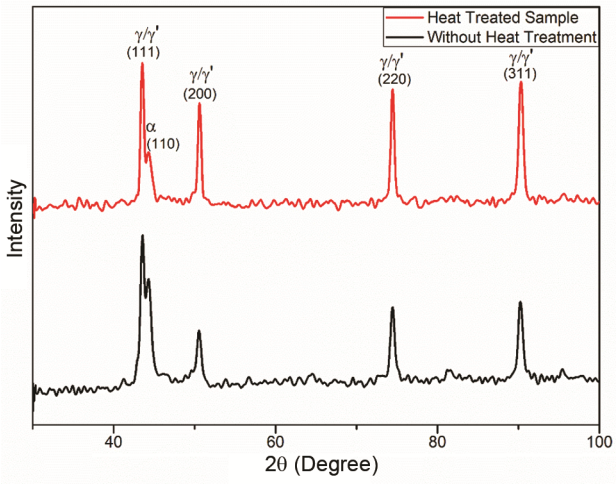

Fig. 14 — XRD graph of welded and heat-treated welded sample.

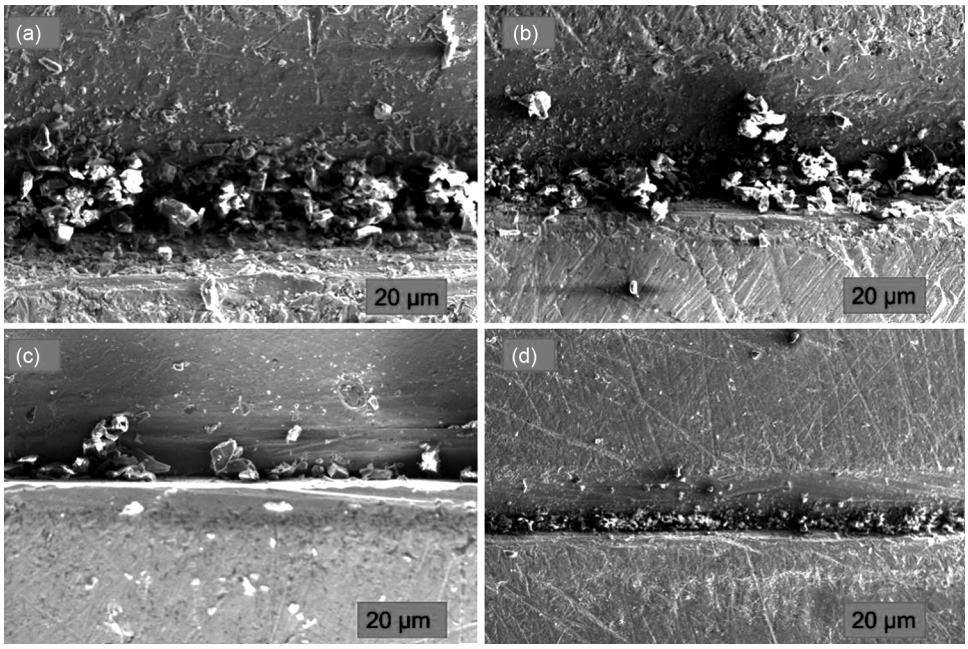

Fig. 15 — SEM image of welded and heat-treated welded sample (a) & (b) welded sample, (c) & (d) heat treated welded sample.

4 Conclusion

Property evaluation and comparison of Micro plasmabutt welded joints of 0.5 mm SS304 sheets are carried out with and without post weld heat treatment (PWHT) by microstructure, hardness, tensile test, X-Ray diffraction (XRD) and scanning electron microscope (SEM). Furthermore, optimization of the process parameter for sound welding using ANN tool is accomplished for maximising the tensile strength. The weld joint at 10 Ampere, 3.5 Lpm and 4.2 mm/sec is calculated to have the maximum tensile strength. At this optimized parameter, the welded sample is undergonepost heat treatment. Hardness value of the heat-treated welded sample is more than that of without heat treated welded sample due to refinement of grain. Formation of the carbides reduced at the fusion region after post heat treatment. Tensile strength of welded sample before and after heat-treatment are 857 MPa and 468 MPa respectively.

Acknowledgment

The authors wish to acknowledge the financial support provided by the Ministry of Education (India) through National Institute of Technology Jamshedpur, grant number O.O.NO.NITJSR/ACAD/2020/16 for conducting the research work. The authors also acknowledge IIT Kharagpur for SEM and XRD facilities, and ASR Metallurgy Jamshedpur for optical microscopy (OM), heat treatment, microhardness, and tensile test.

References

1 Baruah M and Bag S, *Weld World,* 61 (2017) 857.
2 Arunkumar M, Dhinakaran V, Sivashanmugam N and Petley V, *Mater Res,* 22 (2019)
3 Batool S, Khan M, Jaffery S H I, Khan A, Mubashar A, Ali L, Khan N and Anwar M N, *Proc Inst Mech Eng Part L J Mater Des Appl,* 230 (2016) 1005.
4 Li J, Sun Q, Liu Y, Zhen Z, Sun Q and Feng J, *J Manuf Process,* 50 (2020) 629.
5 Aghayar Y, Naghashzadeh A R and Atapour M, *Vacuum,* 184 (2021) 109970.
6 Errico V, Campanelli S L, Angelastro A, Mazzarisi M and Casalino G, *J Manuf Process,* 56 (2020) 96.
7 Chaki S, *SN Appl Sci,* 1 (2019) 1.
8 Akhyar, Tamlicha A, Farhan A, Azwinur, Syukran, Fadhilah T A, Firsa T and Raja Ghazilla R A, *Sustainability,* 14 (2022) 1405.
9 Saha D and Pal S, *J Mater Eng Perform,* 28 (2019) 2588.
10 Chaudhary J, Jain N K Pathak S and Koria S C, *J Micromanufacturing,* 2 (2019) 15.
11 Ramkumar K D, Ramanand R, Ameer A, Simon K A and Arivazhagan N, *Mater Sci Eng A,* 658 (2016) 326.
12 Lin CM, Huang CZ, Su CY and Chen CS, *Mater. Lett,* 204 (2017) 89.
13 Panov D, Naumov S, Stepanov N, Sokolovsky V, Volokitina E, Kashaev N, Ventzke V, Dinse R, Riekehr S, Povolyaeva E, Nochovnaya N, Alekseev E, Zherebtsov S and Salishchev G, *Intermetallics,*143 (2022)
14 Haigen J, Kemou X, Xiaomei Y and Chengji M, *Metallogr Microstruct Anal,*10 (2021) 410.
15 Szusta J, Tüzün N and Karakaş, *Theor Appl Fract Mech,* 100 (2019) 27.
16 Kuril A A, Jagannatham M, Janaki Ram G D and Bakshi S R, *Metallogr Microstruct Anal,* 8 (2019) 848–860.
17 Fatima S, Khan M, Jaffery S H I, Ali L, Mujahid M and Butt S I, *Proc Inst Mech Eng. Part L J Mater Des Appl,* 230 (2016) 640.